Dynamic Interactions of Cortactin and Membrane Type 1 Matrix Metalloproteinase at Invadopodia: Defining the Stages of Invadopodia Formation and Function

Vira V. Artym,[1,3] Ying Zhang,[2] Françoise Seillier-Moiseiwitsch,[2] Kenneth M. Yamada,[3] and Susette C. Mueller[1]

[1]Department of Oncology and [2]Division of Biostatistics and Bioinformatics, Lombardi Comprehensive Cancer Center, Georgetown University Medical School, Washington, District of Columbia; and [3]Craniofacial Developmental Biology and Regeneration Branch, National Institute of Dental and Craniofacial Research, NIH, Bethesda, Maryland

Abstract

Metastatic tumor cells that actively migrate and invade surrounding tissues rely on invadopodia to degrade extracellular matrix (ECM) barriers. Invadopodia are membrane protrusions that localize enzymes required for ECM degradation. Little is known about the formation, function, and regulation of invadopodia. Here, we show that invadopodia have two distinct aspects: (*a*) structural for organizing the cellular actin cytoskeleton to form membrane protrusions and (*b*) functional for using proteolytic enzyme(s) for ECM degradation. Small interfering RNA (siRNA) inhibition established that organization of invadopodia structure requires cortactin, whereas protease inhibitor studies identified membrane type 1 matrix metalloproteinase (MT1-MMP) as the key invadopodial enzyme responsible for gelatin matrix degradation in the breast carcinoma cell line MDA-MB-231. The inhibition of invadopodial structure assembly by cortactin depletion resulted in a block of matrix degradation due to failure of invadopodia formation. Either protease inhibition or MT1-MMP siRNA depletion moderately decreased the formation of invadopodial structures that were identified as actin-cortactin accumulations at the ventral cell membrane adherent to matrix. The invadopodia that were able to form upon MT1-MMP inhibition or depletion retained actin-cortactin accumulations but were unable to degrade matrix. Examination of cells at different time points as well as live-cell imaging revealed four distinct invadopodial stages: membrane cortactin aggregation at membranes adherent to matrix, MT1-MMP accumulation at the region of cortactin accumulation, matrix degradation at the invadopodia region, and subsequent cortactin dissociation from the area of continued MT1-MMP accumulation associated with foci of degraded matrix. Based on these results, we propose a stepwise model of invadopodia formation and function. (Cancer Res 2006; 66(6): 3034-43)

Introduction

Proteolytic degradation of extracellular matrix (ECM) is a critical step in tumor cell invasion (1). Invadopodia are specialized membrane protrusions of invading tumor cells that extend into the ECM and mediate cellular digestion of, and invasion through, the ECM (2, 3). At the ultrastructural level, invadopodia are filament-like protrusions of the ventral cell membrane adherent to matrix that can range from 0.1 to 0.8 μm in diameter and reach >2 μm in length (2, 4). Recent studies based on correlative light electron microscopy show that invading tumor cells at sites of ECM degradation form complex superstructures: cell membrane invaginations 8 μm wide and 2 μm deep containing multiple slender invadopodial protrusions (5). Multiple proteins are associated with invadopodia and can be classified into four major functional groups (for review, see ref. 6). The first group is a minimal motility machine that includes actin and regulators of filamentous actin (F-actin) polymerization/branching (7). Among these are Arp2/3, N-WASP, Cdc42, Nck, cofilin, capping proteins, cortactin, and dynamin. The second group includes adhesion proteins, such as multiple integrins, that mediate invadopodia interaction with ECM. The third group comprises signaling proteins that regulate the actin cytoskeleton and membrane remodeling (tyrosine kinases and Ras-related GTPases). Membrane-associated proteases mediating ECM degradation at sites of invadopodia function constitute the fourth group. Among them are membrane type 1 matrix metalloproteinase (MT1-MMP), seprase, MMP-2, and the urokinase-type plasminogen activator (uPA)/uPA receptor proteolytic system (8–13).

It is generally accepted that the formation of cell protrusions is driven by actin polymerization at the leading edge. Indeed, it has been established that an N-WASP–Arp2/3–cortactin–dynamin complex is essential for invadopodia formation (4, 5, 14). Although invadopodia contain a variety of proteins, specific molecular markers unique to invadopodia have not been identified. Little is known about mechanisms of formation, function, and regulation of invadopodia. Therefore, to dissect the dynamic mechanisms that govern the formation and function of invadopodia, we have focused on two proteins, one of which allows the monitoring of cytoskeletal changes at invadopodia and another that yields information on the ECM-degrading function of invadopodia. These proteins are cortactin and MT1-MMP.

Cortactin, an actin-binding protein, has diverse cellular functions (for review, see refs. 15, 16). Its acidic NH_2-terminal domain mediates cortactin binding to the Arp2/3 complex, promoting actin filament branching and stabilization of branched networks (17). Internal to the acidic NH_2-terminal domain is the cortactin repeat region followed by a α-helical domain, a proline-rich domain with regulatory serine/threonine and tyrosine phosphorylation sites, and a Src homology 3 domain at the COOH terminus. The cortactin repeats mediate cortactin binding to F-actin. The cortactin Src homology 3 domain binds to a variety of targets providing a link

Note: Supplementary data for this article are available at Cancer Research Online (http://cancerres.aacrjournals.org/).

Requests for reprints: Susette C. Mueller, Department of Oncology, Lombardi Comprehensive Cancer Center, Georgetown University, E301 Research Building, Box 571469, Washington, DC 20057-1469. E-mail: muellers@georgetown.edu.

doi:10.1158/0008-5472.CAN-05-2177

between specific transmembrane receptors and the underlying actin cytoskeleton as well as recruiting particular binding proteins to regions of cortical actin and playing a role in a variety of vesicle transport pathways (16, 18). Cortactin is a target for phosphorylation by tyrosine and serine/threonine kinases (19). Differential regulation of cortactin by cellular kinases that effect cortical actin polymerization makes cortactin an important regulatory point. Moreover, the human gene *EMS1* coding for cortactin is overexpressed in 13% of breast carcinomas and 29% of head and neck tumors, mainly due to gene amplification (20). Its overexpression in cells enhances cell migration, invasion, and tumor cell metastasis (21–24).

MT1-MMP is a membrane-bound metalloproteinase with broad substrate specificity and multiple cellular functions. MT1-MMP degrades multiple ECM components, including collagen types I, II, and III; fibronectin; and laminins 1 and 5 (for a review, see ref. 25). Furthermore, MT1-MMP increases the range of proteolytic activities by activating MMP-2 and possibly MMP-13. In addition, MT1-MMP may proteolytically modify CD44, α_V integrin, and transglutaminase, thereby exerting regulatory effects on cell migration (25). MT1-MMP activity is crucial for both physiologic processes and the progression of cancer (26, 27). It is highly expressed in different invasive cancers. MT1-MMP overexpression in cancer cells promotes cell migration, invasion, and metastasis *in vitro* and *in vivo* (25, 28, 29). In invasive tumor cell lines, MT1-MMP invadopodial localization requires membrane anchorage of the enzyme and its expression in cancer cells increases cell invasion by stimulating invadopodial activity (10).

Here, we show that both cortactin and MT1-MMP are required for the assembly of functional invadopodia that degrade gelatin matrix in invasive MDA-MB-231 carcinoma cells. Cortactin is necessary for the maintenance of F-actin-enriched invadopodial core structures. In the presence of functional MT1-MMP, actin-cortactin aggregates of invadopodia support MT1-MMP accumulation at invadopodia required for initiation and sustenance of matrix degradation. Depletion of endogenous MT1-MMP levels results in the formation of actin-cortactin structural components of invadopodia that are functionally unable to mediate matrix proteolysis. After the initiation of MT1-MMP accumulation at invadopodia to initiate matrix degradation, cortactin dissociates from invadopodial regions leaving abundant MT1-MMP associated with foci of matrix degradation for continued matrix proteolysis. Based on our results, we propose a stepwise model of invadopodia formation and function.

Materials and Methods

Antibody. Anticortactin 4F11 monoclonal antibody (mAb) was from Upstate (Lake Placid, NY), anti-MT1-MMP AB815 from Chemicon (Temecula, CA), polyclonal anti-Src and anti-phospho-Src pY^{418} antibody from BioSource (Camarillo, CA), and secondary antibody conjugated to Cy2 or Cy5 were from Jackson ImmunoResearch (West Grove, PA).

Cell lines and transfectants. Human breast carcinoma MDA-MB-231 and MCF-7 cell lines were obtained from Tissue Culture Shared Resource of the Lombardi Cancer Center. Cells were maintained in high glucose-DMEM (HyClone, Logan, UT) supplemented with 10% fetal bovine serum (HyClone), 2 mmol/L L-glutamine, 10 units/mL penicillin, and 10 μg/mL streptomycin.

Stable lines of MDA-MB-231 cells transfected with wild-type c-Src, Y527F constitutively active c-Src, and dominant-negative K295R c-Src were a generous gift from Dr. Toshiyuki Yoneda (Department of Medicine, University of Texas Health Science Center at San Antonio, San Antonio, TX; ref. 30).

cDNA vectors and small interfering RNA. Human MT1-MMP in the pEGFPN1 vector (BD Biosciences Clontech, Palo Alto, CA) was a kind gift from Drs. Henning Birkedal-Hansen and Sarah Netzel-Arnett (National Institute of Dental and Craniofacial Research, NIH, Bethesda, MD; ref. 31). Stable cell populations expressing MT1-MMP enhanced green fluorescent protein (MT1-MMP-eGFP) were generated from parental MDA-MB-231 and Y527F c-Src cells.

Human cortactin cDNA was purchased from Invitrogen (Carlsbad, CA). Twelve amino acids missing from the actin-binding domain compared with the original sequence (GenBank) was restored by site-directed mutagenesis. Complete cortactin cDNA was cloned into a modified monomeric dsRED pRFP1-C1 vector (BD Biosciences Clontech) that was a kind gift from Dr. Roger Tsien (Department of Pharmacology, University of California at San Diego, San Diego, CA). The cortactin monomeric dsRED [cortactin-mRFP(1)] vector was stably expressed in MDA-MB-231 cells stably expressing MT1-MMP-eGFP. Stable cell populations expressing MT1-MMP-eGFP as well as MT1-MMP-eGFP and cortactin-mRFP(1) were selected based on three consecutive sortings for eGFP and mRFP fluorescence with a Becton Dickinson FACStarPlus system (Becton Dickinson, Franklin Lakes, NJ).

Pools of four small interfering RNA (siRNA) duplexes each were designed to target human cortactin (accession no. NM_138565; Qiagen, Valencia, CA) or human MT1-MMP (accession no. NM_004995; Dharmacon, Lafayette, CO). As a negative control, cells were transfected with nonspecific siRNA pool (Dharmacon). All cDNA vectors and siRNA transfections were done with Lipofectamine 2000 (Invitrogen) according to the instructions of the manufacturer.

Fluorescent-gelatin degradation assay. Gelatin was conjugated with AlexaFluor (Molecular Probes, Eugene, OR) using the protocol of the manufacturer. Coverslips (18 mm) were precleaned with 20% nitric acid for 30 minutes followed by extensive washing. Ethanol-sterilized coverslips were coated with 50 μg/mL poly-L-lysine for 20 minutes at room temperature, washed with PBS, and fixed with 0.5% glutaraldehyde for 15 minutes followed by extensive washing. Then, the coverslips were inverted on an 80 μL drop of gelatin matrix (0.2% gelatin and AlexaFluor-gelatin at an 8:1 ratio) and incubated for 10 minutes at room temperature. After washing with PBS, the residual reactive groups in the gelatin matrix were quenched with sodium borohydride at 5 mg/mL for 15 minutes followed by extensive washing with PBS.

To assess the ability of cells to form invadopodia and degrade matrix, cells were plated on coverslips coated with fluorescent gelatin matrix in 12-well plates at 4×10^3/mL and incubated at 37°C. Foci of degraded matrix were visible as dark areas ~0.2 to 1.2 μm in diameter that lack fluorescence and appear as "holes" in the bright fluorescent gelatin matrix. A cell degrading at least one hole under the cell or near the cell edge was counted as a cell able to degrade matrix. For image presentation, MetaMorph (Molecular Devices, Sunnyvale, CA) median (2 × 2) filter was applied to fluorescent images of the matrix.

Immunocytochemistry. Cells were fixed-permeabilized with 3.7% formaldehyde/0.1% Triton X-100 for 10 minutes, washed with PBS, and labeled with 10 μg/mL primary antibodies for 1 hour followed by labeling with secondary fluorochrome-conjugated antibodies for 30 minutes. Actin filaments were visualized with Alexa-phalloidin (Molecular Probes).

Confocal fluorescence microscopy. Confocal images were collected using a Zeiss510-META laser scanning confocal microscope (Carl Zeiss, Thornwood, NY) with Zeiss Plan-Neofluar 100×/1.3 N.A. oil or Plan-Apochromat 63×/1.4 N.A. oil objectives. For optimal confocality, all images were collected with the pinhole photodetector aperture set equal or <1 Airy unit. Images were processed with AutoDeBlur (AutoQuant Imaging, Watervliet, NY) two-dimensional or three-dimensional blind deconvolution using a total of 30 iterations.

Live fluorescence microscopy. Live cells expressing eGFP and mRFP protein chimeras were imaged with a Zeiss Axiovert200M microscope equipped with an UltraVIEW-RS confocal live-cell imager (Perkin-Elmer, Boston, MA) with a Zeiss Plan-Apochromat 63×/1.4 N.A. oil objective. An environmental chamber mounted on the microscope maintained constant 37°C temperature, CO_2, and humidity. For live fluorescence microscopy, cells were seeded in microwell dishes (MatTek, Ashland, MA) with glass bottoms coated with fluorescent-gelatin matrix as described above. To suppress formation of cytotoxic free radicals, Oxyrase (Oxyrase, Mansfield, OH) was added at a 1:100 dilution to culture medium immediately before cell imaging.

Transmission electron microscopy. Cells at 5×10^5/mL in complete culture medium were incubated in glass-bottom dishes coated with Gelatin-Alexa568 matrices for 3 hours. Cells were fixed with 2.5% glutaraldehyde/2% paraformaldehyde for 2 hours, postfixed in 1% osmium tetroxide for 1 hour, *en bloc* stained with uranyl acetate, and processed for conventional ultrathin section electron microscopy as described previously (4). Layers of plastic-embedded cells on matrix were removed from the coverslips, reembedded in plastic, and sections were cut perpendicular to the original plane of the coverslip. Sections were poststained with uranyl acetate and lead citrate, and photographed with a Hitachi H-7600 transmission electron microscope.

Immunoblotting. Cells cultured overnight at 2×10^5/mL in six-well plates were extracted with radioimmunoprecipitation assay buffer, mixed with sample buffer containing β-mercaptoethanol, sonicated, and boiled for 5 minutes. SDS-PAGE was done using 4% to 12% Tris-glycine gels (Novex, Invitrogen). Semiquantitative analysis of protein levels was done using ScionImage software (Scion, Frederick, MD).

Biotinylation and immunoprecipitation. Cell surface protein biotinylation and immunoprecipitation to identify surface MT1-MMP was done as described (32).

Gelatin zymography. Cells at 3×10^5 per well in six-well plates were incubated overnight. For culture medium samples, cells were cultured in serum-free DMEM for 48 hours. Cells were lysed with 1% NP40 in 10 mmol/L Tris (pH 7.4), 150 mmol/L NaCl, 1 mmol/L $CaCl_2$, and 1 mmol/L $MgCl_2$. To detect MMP-2 activity, cell culture medium and cell lysates were concentrated six times and twice, respectively, by filtration on Microcon filter devices (Millipore, Billerica, MA). Samples were mixed with sample buffer without reducing agent, incubated for 10 minutes at room temperature, and separated on 10% polyacrylamide/0.1% gelatin gels. Then, gels were extensively washed in 2.5% Triton X-100 and incubated in 50 mmol/L Tris-HCl (pH 7.5), containing 0.2 mol/L NaCl, 5 mmol/L $CaCl_2$, 1 μmol/L $ZnCl_2$, 0.02% Brij 35, and 1 mmol/L *p*-aminophenylmercuric acetate at 37°C for 36 hours. The gel was stained with 0.5% Coomasie blue R-250. Gel loadings were normalized to total protein measured with a micro-BCA kit (Pierce, Rockford, IL).

Real-time PCR. MMP expression levels were measured by quantitative real-time PCR (qRT-PCR). Cells plated in six-well plates at 2×10^5/mL were cultured overnight, then mRNA was collected using the RNAaqueous 4-PCR kit (Ambion, Austin, TX). cDNA was synthesized using a GeneAmp reverse transcription reaction kit (Applied Biosystems, Foster City, CA). qRT-PCR was carried out with SYBR green PCR master mix (Applied Biosystems) using an ABI Prism7700 Sequence detector (Perkin-Elmer). Thermal cycling variables for the qRT-PCR were 50°C for 2 minutes, 95°C for 10 minutes, 40 cycles of denaturation at 95°C for 15 seconds, and annealing/extension at 65°C for 30 seconds. The primers for human MMPs and internal controls used for RT-PCR are provided in Supplementary Fig. S1*A*. The results were presented as fold change in gene expression.

Statistical analysis. The data are represented graphically as a mean value with the corresponding SD, calculated after pooling three independent trials. For comparison between groups, *t* test was used. For analysis of live-cell imaging data, the sign and Wilcoxon signed-rank (two-sided) test were applied for pairwise comparisons between groups.

Results

Elevated levels of c-Src stimulate ECM degradation via increased invadopodia formation. To study invadopodial dynamics, we searched for a cell line with a high percentage of cells capable of degrading matrix with significant numbers of invadopodia per cell. Because c-Src increases cell invasive potential (30, 33–37), we investigated the effect of c-Src expression on gelatin degradation by the breast carcinoma cell line MDA-MB-231 as a cell model. Degradation assays involved culturing cells on coverslips coated with thin, fluorochrome-conjugated gelatin matrices that were not cross-linked with glutaraldehyde (see Materials and Methods). Local proteolytic activity was identified by appearance of dark areas lacking fluorescence in the bright fluorescent matrix. According to electron microscopy, the thickness of our matrices is 48.9 ± 2.9 nm (Fig. 1*D, inset*). Unlike widely used glutaraldehyde cross-linked fluorescent gelatin films, the fluorescent matrices that we developed provide better sensitivity, allowing precise detection of local cell proteolytic activity after short incubation periods.

Incubation of parental carcinoma cells and cells expressing wild-type c-Src as well as mutant Y527F c-Src and K295R c-Src on fluorescent gelatin matrixes for different periods of time detected differences in numbers of cells degrading matrix (Fig. 1*A*). The percentage of parental carcinoma cells able to degrade the matrix gradually increased with time and reached ~20% upon 3 hours of incubation. Elevated levels of wild-type c-Src or Y527F c-Src in these cells stimulated matrix degradation as detected by increases in the percentage of cells degrading matrix over time (Fig. 1*A*). Increased cellular Src conferred ability to ~40% of the cells to degrade the gelatin matrix by 3 hours, whereas expression of Y527F c-Src increased the percentage to 55% (Fig. 1*A*).

Matrix degradation by cancer cells is mediated by invadopodia. Calculation of the mean number of invadopodia per cell showed substantial increases in formation of invadopodia with elevations in wild-type c-Src and dominant-active c-Src levels (Fig. 1*A* and *D*). Specifically, the mean number of invadopodia in our cell lines quadrupled after augmentation of c-Src levels compared with parental carcinoma cells, and it increased nearly 7-fold with expression of Y527F c-Src. The expression of K295R c-Src decreased the mean number of invadopodia per cell by ~65% compared with parental cell line. Because Src induced a high percentage of cells capable of cleaving gelatin matrix by forming abundant invadopodia, we chose wild-type c-Src and Y527F c-Src MDA-MB-231 cells as convenient models to study the mechanisms of invadopodia formation and function in depth.

We also examined the effect of Y527F c-Src on expression and activity of several MMPs capable of gelatin degradation. Quantitative RT-PCR detected increases in MT1-MMP and MMP-9 mRNA expression levels of 1.4- and 16-fold, respectively, in carcinoma cells expressing Y527F c-Src compared with parental (Fig. 1*B*). No effects were observed on the mRNA expression levels of MMP-2, MMP-13, MMP-15, or MMP-16. The increase in MT1-MMP mRNA expression level correlated with the increase in amount of cell surface MT1-MMP in Y527F c-Src cells (Fig. 1*B*). Gelatin zymography of cell culture medium and cell lysates detected elevated levels of pro-MMP-9 (92 kDa) in Y527F c-Src–expressing cells (Fig. 1*C*), consistent with qRT-PCR data. The active 86 kDa form of MMP-9 appeared only in cell lysates and was elevated in Y527F c-Src cells. Gelatin zymography detected only pro-MMP-2 (72 kDa) in both cell lysates and culture medium with no difference in pro-MMP-2 levels in Y527F c-Src cells compared with parental cells (Fig. 1*C*).

Cortactin is indispensable for invadopodia formation. Early studies on invadopodia revealed that microinjection of anticortactin polyclonal antibodies decreased the number of matrix-degrading cells (4). To assess the role of cortactin in the dynamics of formation and function of invadopodia, we implemented a siRNA-targeted protein depletion approach. Based on dose dependence analysis using parental MDA-MB-231 to obtain ~90% suppression of cortactin levels (Supplementary Fig. S1*B*), we treated parental, wild-type c-Src, and Y527F c-Src MDA-MB-231 cells with 80 nmol/L cortactin-specific pools of four siRNAs for 72 hours (Fig. 2*A*).

Cortactin depletion decreased cell migration on gelatin matrices (Supplementary Fig. S1*C*) and inhibited matrix degradation

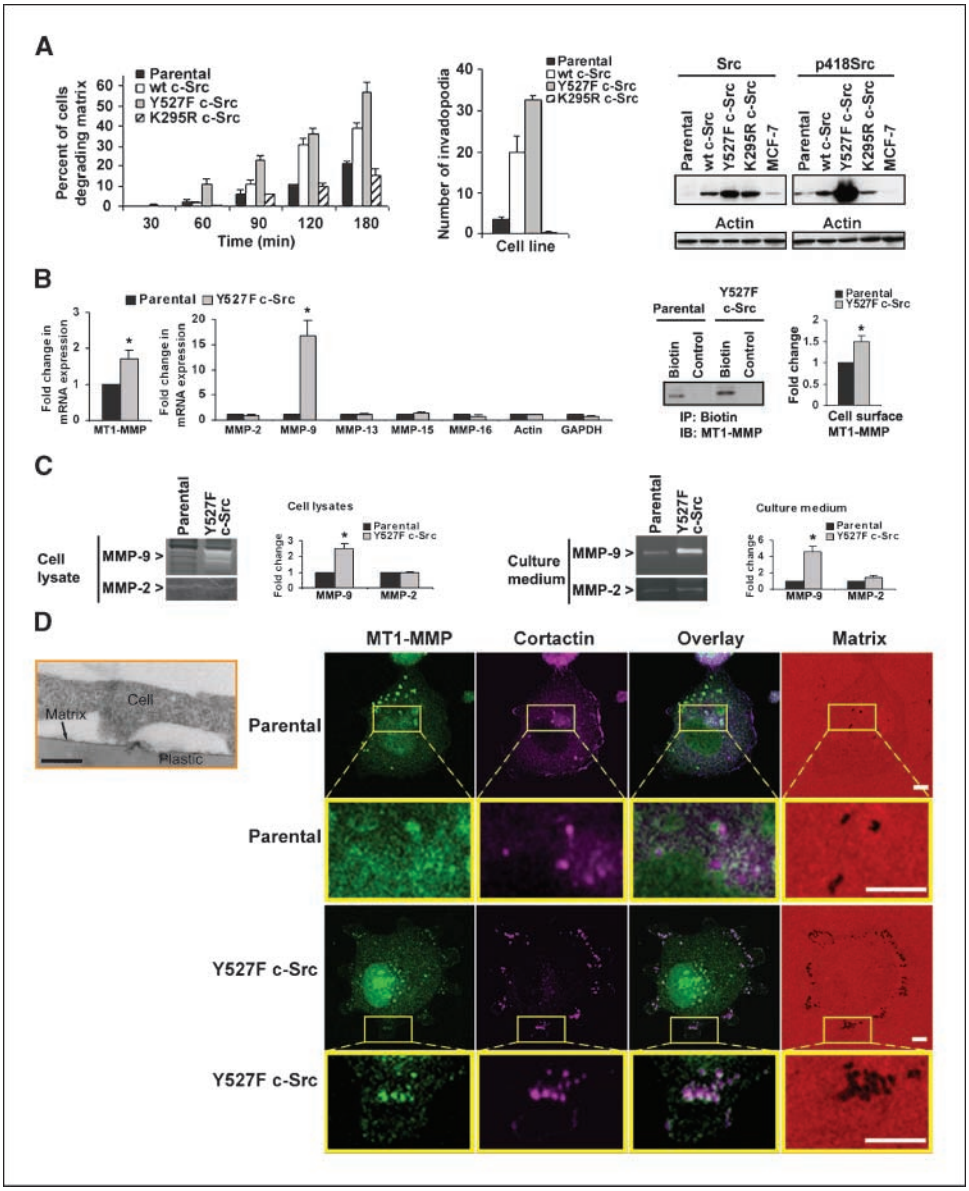

Figure 1. Expression of wild-type c-Src or constitutively active c-Src increases cellular degradation of fluorescent matrix by stimulating invadopodia formation. *A,* effect of c-Src expression on the ability of cells to degrade gelatin matrix and form invadopodia. Parental, wild-type c-Src, and mutant Y527F c-Src and K295R c-Src–expressing MDA-MB-231 cells were incubated on Alexa568-labeled gelatin matrices for the indicated times. Cells degrading fluorescent matrix were identified by the appearance of dark areas ("holes") at the sites of degraded fluorescent gelatin. The cell was counted as degrading matrix if at least one hole was identified under the cell body or in immediate proximity to the cell. To characterize the effect of c-Src and mutant c-Src expression on invadopodia formation, parental, wild-type c-Src, and c-Src mutant clones of MDA-MB-231 cells were incubated on Alexa568-gelatin matrices for 3 hours. After incubation, the cells were fixed, permeabilized, and stained for cortactin and MT1-MMP. Invadopodia were identified by colocalization of cortactin and MT1-MMP staining over a site of degraded matrix (hole). Representative Western blots show levels of Src and tyrosine phosphorylated Src (p418Src) in parental, wild-type c-Src, Y527F c-Src, and K295R c-Src MDA-MB-231 clones. The breast carcinoma cell line MCF-7, which is not able to cleave fluorescent gelatin matrices, was used as a negative control. *B,* quantitative RT-PCR analysis of the effect of Y527F c-Src expression on mRNA levels of gelatin-degrading MMPs in breast carcinoma cells. *, significant increase compared with parental ($P < 0.01$). The increase in MT1-MMP mRNA expression in Y527F c-Src cells correlates with the elevation in cell surface MT1-MMP measured by immunoprecipitation of biotinylated cell surface MT1-MMP. *IP,* immunoprecipitation; *IB,* immunoblotting. *, significant increase compared with parental ($P < 0.05$). *C,* elevated activity of MMP-9 but not MMP-2 detected by gelatin zymography of cell lysates and cell culture medium of carcinoma cells stably expressing Y527F c-Src. *, significant increase compared with parental ($P < 0.01$). *D,* representative micrographs of parental and Y527F c-Src–expressing MDA-MB-231 cells incubated on gelatin-Alexa568 matrices for 3 hours. After fixation, cells were immunolabeled for MT1-MMP (primary AB815 followed by secondary Cy-2 conjugated antibody) and cortactin (primary 4F11 antibody followed by secondary Cy-5 conjugated antibody). *Dark dot-like regions on bright fluorescent matrix* are the foci of pericellular proteolysis mediated by the invadopodia. Invadopodia are identified as a colocalization of cortactin and MT1-MMP immunostaining with the foci of degraded matrix. Bars, 5 μm. Electron microscopy (*inset*) shows the thickness and consistency of the fluorescent gelatin-Alexa568 matrix. Bar, 500 nm.

(Fig. 2*B*). To evaluate the ability of cells to form invadopodia under conditions of depleted cortactin, the cells were immunolabeled for actin and cortactin (Fig. 2*C*). In the control cells, the majority of actin-cortactin aggregates were associated with sites of degraded matrix after 3 hours of incubation on the gelatin matrix, indicating that functional invadopodia were formed. Depletion of cellular cortactin inhibited formation of the actin-cortactin aggregates and was accompanied by strong inhibition of matrix degradation (Fig. 2*B* and *C*). These results indicate that cortactin is required for formation of invadopodia and they suggest that the inhibition of

matrix proteolysis by cells with depleted cortactin is caused by the impairment of invadopodia formation.

MT1-MMP is required for invadopodia function but not for invadopodia initiation. Several proteases have been shown to be associated with invadopodia of cancer cells. In our cell model, Y527F c-Src expression stimulated MT1-MMP and MMP-9 expression. To establish which proteases are responsible for gelatin matrix degradation in MDA-MB-231 carcinoma cells, we tested the effect of different protease inhibitors on matrix degradation (Fig. 3). Only tissue inhibitor of metalloproteinase (TIMP)-2, an inhibitor of soluble and membrane-bound MMPs, including MT1-MMP, was able to suppress matrix degradation at 0.3 μg/mL (Fig. 3*A* and *D*) and completely inhibited at 3 μg/mL (data not shown). In contrast, TIMP-1, which inhibits soluble MMPs but not membrane-type MMPs, did not reduce gelatin matrix degradation. Nevertheless, immunostaining of the TIMP-2-treated cells still revealed association of actin-cortactin aggregates with the cell membrane adherent to nondegraded matrix. These aggregates were identical in appearance and location to those in invadopodia of control cells. In wild-type c-Src and Y527F c-Src cells treated with TIMP-2, the total numbers of actin-cortactin aggregates were ~40% and ~30% less than those of the control, respectively (Fig. 3*A*).

Similar results were obtained upon carcinoma cell transfection with siRNA targeting MT1-MMP gene expression (Fig. 3*B, C*, and *D*). By suppressing MT1-MMP expression, we observed strong inhibition of matrix degradation by parental, wild-type c-Src, and Y527F c-Src–expressing cells. However, the formation of actin-cortactin structures was only modestly reduced (60-70% remained). Thus, we conclude that onset of invadopodia formation is independent of MT1-MMP, whereas the matrix-degrading capacity of invadopodia requires availability of catalytically functional MT1-MMP. Furthermore, matrix degradation of fluorescent type I collagen matrices by Y527F c-Src cells was observed at invadopodia (data not shown), further implicating MT1-MMP in invadopodia function.

Cortactin and MT1-MMP association at invadopodia is sequential. Given the conclusion that cortactin and MT1-MMP are essential components of functional invadopodia in MDA-MB-231 carcinoma cells capable of gelatin matrix degradation, we closely examined cells immunostained for cortactin and MT1-MMP (Fig. 4*A*). The cells revealed four distinct patterns of protein accumulation and matrix degradation: accumulations of

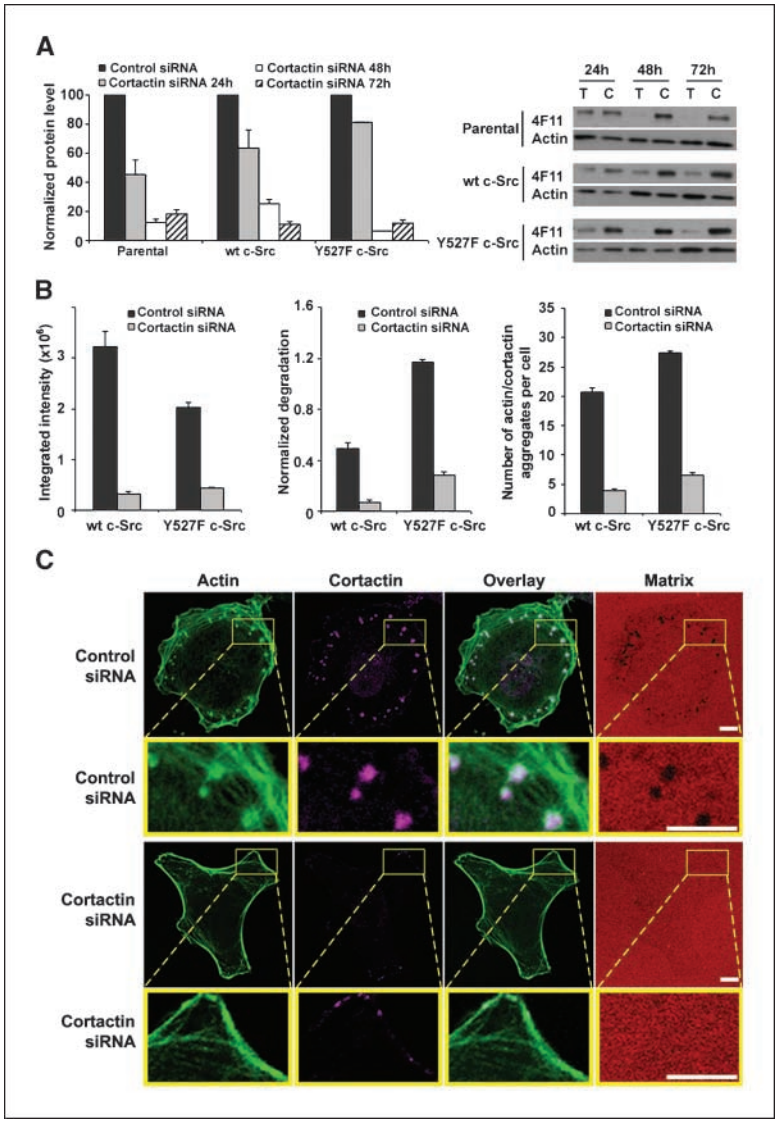

Figure 2. Inhibition of cortactin expression blocks matrix degradation by carcinoma cells as a result of down-regulation of invadopodia formation. *A,* cortactin levels at different time points after transfection of cells with cortactin-specific siRNA. Parental, wild-type c-Src, and Y527F c-Src–expressing MDA-MB-231 cells were transfected with 80 nmol/L siRNA pool targeting cortactin (*Cortactin siRNA*) or 80 nmol/L nonspecific siRNA pool as a control (*Control siRNA*). Cell lysates were collected at 24, 48, and 72 hours posttransfection. Cortactin protein levels were calculated based on densitometric analysis of Western blots and normalized to the cortactin level of the siRNA control. Representative Western blot shows cortactin levels (anticortactin 4F11 antibody staining) for cortactin-specific siRNA-treated (*T*) and control siRNA-treated (*C*) cells at different time points. *B,* effect of cortactin-specific siRNA on cellular level of cortactin, ability of the cells to degrade matrix, and number of actin/cortactin aggregates per cell. Cortactin levels in the cells were determined as the integrated intensity of cortactin immunostaining of cells treated with cortactin-specific siRNA or control siRNA. Cellular capacity to degrade matrix is represented as normalized degradation, which was calculated as the area of degraded matrix normalized to the total area of adherent cell membrane per cell. The number of actin/cortactin aggregates per cell, which is used to represent the degree of invadopodia formation, was calculated as the mean number of immunofluorescently labeled actin and cortactin aggregates that colocalized. *C,* representative micrographs of Y527F c-Src–expressing MDA-MB-231 cells transfected with cortactin-targeting siRNA or control siRNA and plated on gelatin-Alexa568 matrices at 72 hours posttransfection. The cells were incubated on gelatin matrices for 3 hours. Immunolabeling was done for actin with phalloidin-Alexa488 and cortactin with primary 4F11 antibody and secondary Cy5-conjugated antibody. Bars, 5 μm.

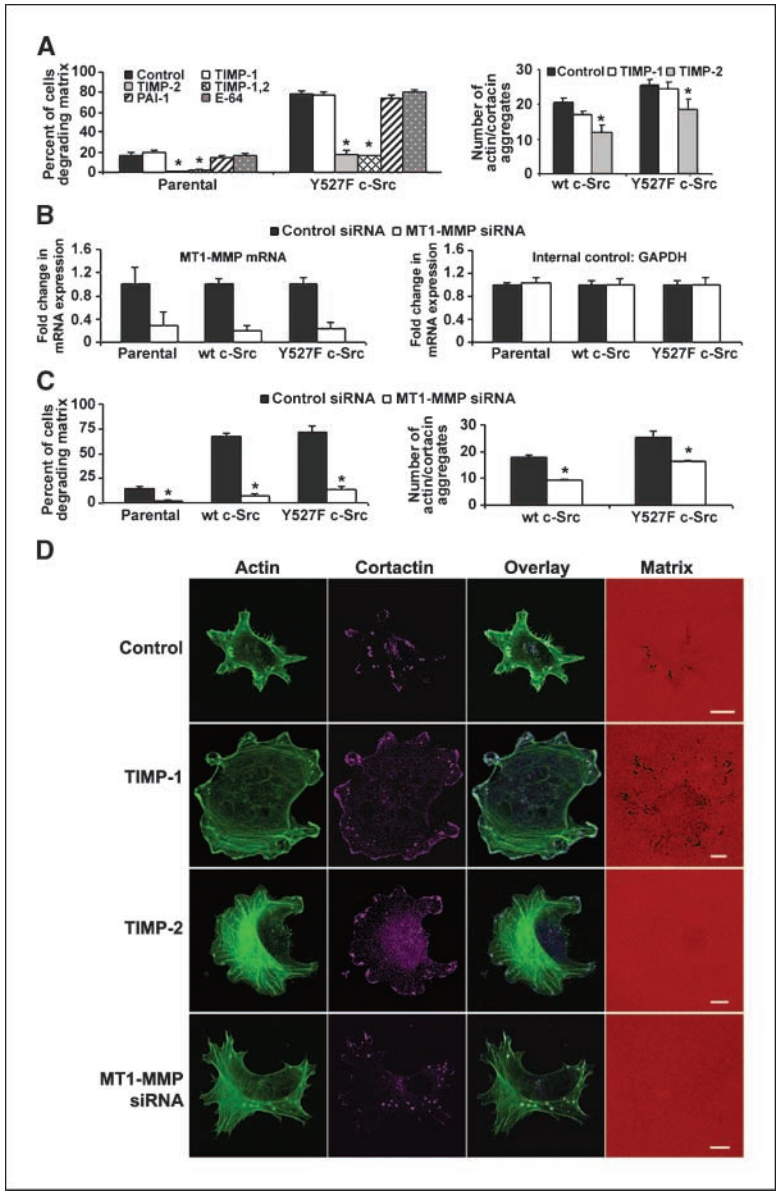

Figure 3. Inhibition of MT1-MMP protease activity of carcinoma cells inhibits matrix degradation by the cells, whereas invadopodia formation is affected only modestly. *A,* effect of protease inhibitors on matrix degradation by parental and Y527F c-Src MDA-MB-231 cells and formation of invadopodia. The cells were pretreated with protease inhibitors for 15 minutes and plated on gelatin-Alexa568 matrices in the presence of inhibitors for 3.5 hours. The following protease inhibitors were compared: 0.3 μg/mL TIMP-1, 0.3 μg/mL TIMP-2, combination of 0.3 μg/mL TIMP-1 and 0.3 μg/mL TIMP-2, 10 μg/mL plasminogen activator inhibitor-1 (*PAI-1*), and 100 μg/mL E-64. As a control, cells were treated with PBS. Control and protease inhibitor–treated cells were fixed, permeabilized, and immunolabeled for actin and cortactin. The number of actin-cortactin aggregates near the cell membrane adherent to the gelatin matrix was counted for each treatment (only the data for control, TIMP-1, and TIMP-2 treatments are shown). *, statistically significant decrease compared with control ($P < 0.01$). *B,* changes in MT1-MMP and *glyceraldehyde-3-phosphate dehydrogenase* (*GAPDH*) gene expression after treatment with MT1-MMP-targeted siRNA pool. Parental, wild-type c-Src, and Y527F c-Src MDA-MB-231 cells were treated with 80 nmol/L MT1-MMP-specific siRNA pool (*MT1-MMP siRNA*) or 80 nmol/L nonspecific control siRNA pool (*Control siRNA*). mRNA was extracted at 48 hours after siRNA transfection. The effect of siRNA treatment on mRNA level was assessed by qRT-PCR as fold change in mRNA level. *C,* effect of MT1-MMP-targeted siRNA treatment on matrix degradation and number of actin-cortactin aggregates. Parental, wild-type c-Src, and Y527F c-Src cells at 48 hours after siRNA transfection were plated on gelatin-Alexa568 matrices. Percentage of cells degrading matrix and the number of actin-cortactin aggregates per cell were calculated after 3-hour incubation of cells on gelatin matrix. *, significant decrease compared with control ($P < 0.01$). *D,* representative micrographs of Y527F c-Src–expressing cells treated with TIMP-1 or TIMP-2, or transfected with MT1-MMP-specific siRNA. Cells were incubated on gelatin-Alexa568 matrices for 3 hours, fixed, and labeled for actin (phalloidin-Alexa488) and cortactin (primary 4F11 mAb followed by secondary Cy5-conjugated antibody). Invadopodia are identified as colocalization of actin and cortactin immunostaining with the foci of degraded matrix. Bar, 10 μm.

only cortactin at the cell adherence membrane, cortactin and MT1-MMP aggregation overlying intact matrix, cortactin and MT1-MMP accumulation localized to foci of degraded matrix (single holes), and MT1-MMP association with foci of degraded matrix. These four types of combinations of cortactin and MT1-MMP over intact or degraded matrix were classified as invadopodia stages I, II, III, and IV, respectively.

Next, we examined cortactin and MT1-MMP temporal sequences relative to matrix degradation (i.e., appearance of matrix holes). Y527F c-Src cells stably expressing MT1-MMP-eGFP chimeras were plated on fluorescent matrix and allowed to degrade it for 45 minutes to 3 hours (Fig. 4*B*). After fixation, cells were immunolabeled for cortactin. Figure 4*B* shows the percentage of cell invadopodia at each stage after specific periods of incubation. After 45 minutes of incubation on matrix, ~60% of the invadopodia formed by cells were at stage I, indicating that the initial step of invadopodia formation is linked to cortactin accumulation at the ventral cell membrane adherent to matrix. With time, the number of invadopodia at stage I decreased to ~50% after 1 hour and then 10% after 2 hours of cell incubation on matrix, although it rebounded slightly to ~20% after 3 hours of incubation. The percentage of invadopodia at stage II remained relatively constant (~35%) after short periods of cell incubation on matrix (45 minutes and 1 hour), but then decreased to ~10% with further incubation time. This time course indicates that invadopodial stage II (accumulation of cortactin and MT1-MMP above intact matrix) is relatively short-lived. The number of invadopodia at stages III and IV increased progressively with longer cell incubation on matrix, and after 3 hours, stage IV became dominant. This pattern obviously suggests that upon MT1-MMP accumulation at sites of cortactin aggregates, matrix degradation takes place. Subsequently, cortactin dissociates from the invadopodia, leaving behind MT1-MMP associated with the foci of degraded matrix.

Cortactin is an F-actin-binding protein that associates with the centers of active cortical actin remodeling. To assess the state of F-actin at each of the four invadopodial stages, we did multispectral microscopy of invadopodia (Fig. 4*C*). Y527F c-Src MDA-MB-231 cells stably expressing MT1-MMP-eGFP were plated on fluorescent gelatin matrices for different periods of time. The cells

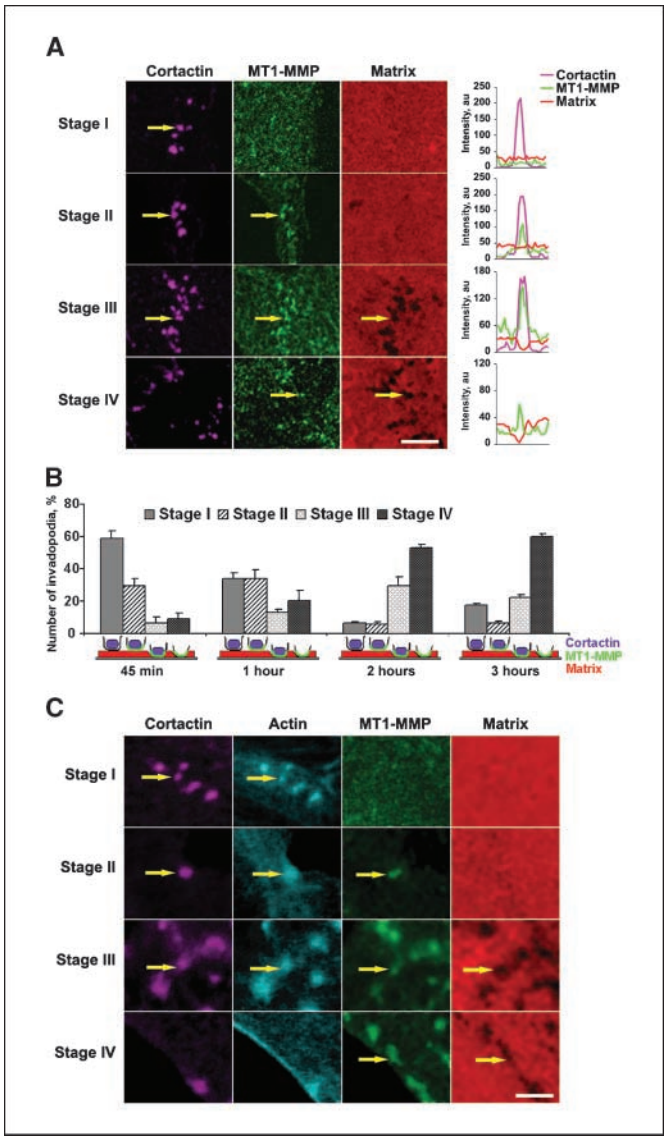

Figure 4. Stages of invadopodia formation and function. *A,* identification of four stages of invadopodia with respect to cortactin and MT1-MMP staining colocalization over intact or degraded matrix. After 3 hours of incubation on the fluorescent gelatin matrix, Y527F c-Src MDA-MB-231 cells were fixed and labeled for cortactin (primary 4F11 followed by secondary Cy-5-conjugated antibody) and MT1-MMP (primary AB815 followed by secondary Cy-2-conjugated antibody). Representative micrographs of each invadopodial stage and the fluorescence intensity profile for anticortactin and anti-MT1-MMP staining as well as gelatin matrix fluorescence are shown. *Bar,* 10 μm. *B,* Y527F c-Src MDA-MB-231 cells stably expressing the MT1-MMP-eGFP chimera were incubated on gelatin-Alexa568 matrices for 45 minutes, 1 hour, 2 hours, or 3 hours. At the end of each incubation period, cells were fixed/permeabilized and immunolabeled for cortactin. Four stages of invadopodia formation were identified: accumulation of cortactin at the adherent cell membrane (stage I), accumulation of cortactin and MT1-MMP over intact matrix (stage II), accumulation of cortactin and MT1-MMP over a site of degraded matrix (stage III), and continued association of MT1-MMP aggregates with the areas of degraded matrix but without cortactin localization (stage IV). *Columns,* percentage of invadopodia per cell present at a particular stage out of the total number of cell invadopodia present (i.e., all stages combined). *C,* representative micrographs of four stages of invadopodia imaged by multispectral laser-scanning microscopy. Y527F c-Src MDA-MB-231 cells stably expressing MT1-MMP-eGFP were incubated on gelatin-Alexa568 matrices for 45 minutes, 1 hour, 2 hours, or 3 hours. At the end of each incubation period, cells were fixed/permeabilized and immunolabeled for cortactin (4F11 antibody followed by Cy5-conjugated secondary staining) and actin (phalloidin-rhodamine, *pseudocolored blue*). Confocal image stacks of gelatin-Alexa568 and phalloidin-rhodamine were acquired at variable emission wavelengths using the META detector. Dye separation was done according to the Zeiss linear unmixing algorithm. Bar, 5 μm.

were then fixed and labeled for cortactin and F-actin. Representative micrographs of invadopodia at each stage are shown in Fig. 4*C*. Cortactin was always associated with F-actin accumulation at invadopodia in stages I, II, and III. The dissociation of cortactin from the invadopodia enriched in MT1-MMP-eGFP at stage IV was accompanied by disappearance of F-actin from that site.

Live-cell imaging reveals the dynamics of stepwise formation of invadopodia and uncovers two types of cortactin association: long lived and short lived. To examine cortactin and MT1-MMP dynamic interactions at invadopodia more extensively and to confirm our proposed four stages of invadopodia formation and function, we turned to live-cell imaging. Three-channel live-cell imaging was used to track the kinetics of matrix degradation by parental carcinoma cells stably expressing MT1-MMP-eGFP and cortactin-mRFP(1) chimeras (Fig. 5). Upon cell adhesion to the fluorescent matrix, dynamic accumulations of cortactin near the ventral cell membrane were observed at multiple sites (data not shown). Some of these cortactin aggregates dispersed whereas others became invadopodia. Invadopodia formation first involved the arrival of a cortactin aggregate to the cell membrane adherent to the matrix, followed by the accumulation of MT1-MMP at the cortactin-rich regions (Fig. 5*A* and *B*; Movies 1 and 2 in Supplementary Data). Accumulation of MT1-MMP at invadopodia was accompanied by high motility of the aggregates of membrane-associated MT1-MMP in and adjacent to invadopodia. The average time for onset of MT1-MMP accumulation at cortactin-rich invadopodia after cortactin initially appeared was 2.25 minutes for migrating cells and 1.5 minutes for nonmigrating cells (Table 1). Accumulation of MT1-MMP at cortactin-containing invadopodial structures resulted in subsequent degradation of matrix underlying the invadopodia. The onset of matrix degradation compared with cortactin arrival at invadopodia was 6 minutes for nonmigrating carcinoma cells and 4.5 minutes for migrating cells (Table 1).

Live-cell imaging also revealed different patterns of cortactin association with invadopodia. In nonmigrating cells, cortactin remained associated with invadopodia for extensive periods of time. Imaging of invadopodia for 90 minutes showed continual presence of cortactin. However, the intensity of this long-lived invadopodial cortactin changed over the 90-minute period (Fig. 5*A, kymograph*). These fluctuations may indicate dynamic actin remodeling at invadopodia. In striking contrast, imaging of carcinoma cells undergoing migration showed short-lived association of cortactin with invadopodia (Fig. 5*B*). In migrating cells, cortactin remained associated with invadopodia for only an average of 10 minutes (median time for cortactin loss from invadopodia is 10.13 minutes; interquartile range is 7.50-20.25 minutes). During this short period of time, invadopodia assembled and matrix degradation was initiated. Cortactin disappearance from the invadopodia resulted in MT1-MMP-enriched but cortactin-free invadopodia that were still able to continue matrix degradation.

Finally, we characterized and compared the relative fluorescence intensities of fluorescently tagged MT1-MMP, cortactin, actin, and matrix to assess relative amounts of each constituent and the extent of matrix proteolysis at each invadopodial stage (Fig. 6*A*). By semiquantitative determinations of pixel intensity integrated over the area of individual invadopodia, the levels of cortactin and actin were confirmed to be initially elevated at stage I. Cortactin and actin levels then rose moderately further at stages II and III, then dropped to zero at stage IV. In contrast, MT1-MMP was absent at stage I and rose sharply to a plateau at stages II to III, and remained high or slightly increased at stage IV. Matrix staining was

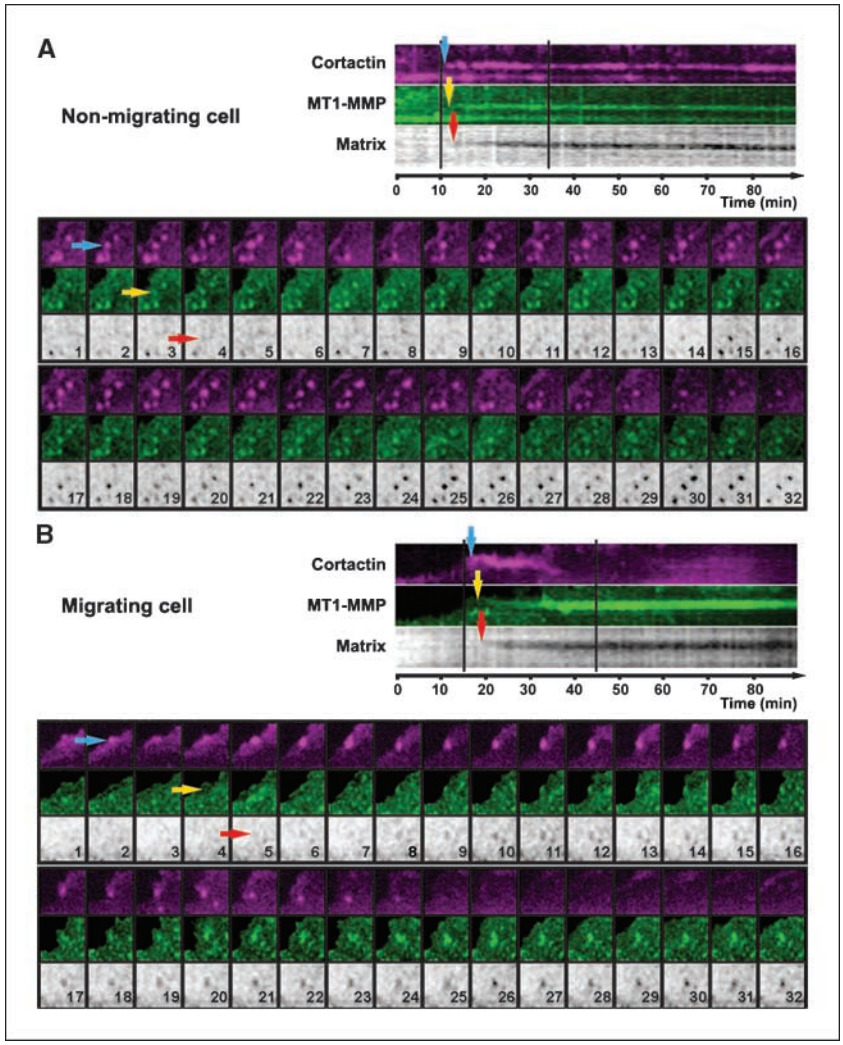

Figure 5. Live-cell imaging of invadopodia reveals the dynamics of assembly and function of invadopodia. *A,* a cell population that stably expresses MT1-MMP-eGFP and cortactin-mRFP(1) was generated from the parental MDA-MB-231 carcinoma line. For live-cell imaging, the cells were plated on gelatin-Alexa647 matrixes and allowed to adhere for 30 minutes. Images of live cells were captured every 45 seconds. Three-channel imaging allowed simultaneous visualization of the dynamics of MT1-MMP-eGFP, cortactin-mRFP(1) at invadopodia compared with local matrix degradation (hole formation). Invadopodia formation and function in nonmigrating (*A*) and migrating (*B*) cells is depicted in the form of kymographs and also as series of 32 consecutive frames that correspond to the range of the kymograph between the two vertical black lines. *Magenta,* cortactin-mRFP(1); *green,* MT1-MMP-eGFP. *Arrows,* onset of cortactin (*blue arrow*), onset of MT1-MMP (*yellow arrow*) accumulation at the invadopodia, and onset of matrix degradation by the invadopodia (*red arrow*).

the opposite: It was highest at stages I and II, then dropped as holes were formed at stage III and IV.

Discussion

Invadopodia are specialized membrane protrusions of invasive tumor cells that mediate focal pericellular proteolysis of ECM and promote tumor cell invasion and metastasis (6). Consequently, understanding the mechanisms governing the formation and function of invadopodia should provide insights into the biology, regulation, and potential therapeutic approaches to cancer metastasis.

In a current view, the induction of invadopodia—F-actin-rich membrane protrusions with matrix degradation activity—is

Table 1. Onset times for MT1-MMP accumulation and matrix degradation relative to initial cortactin accumulation at invadopodia

Cell type	NT*	NI†	MT1-MMP onset, min‡	MT1-MMP onset, interquartile range§	*P* value cortactin vs MT1-MMP	Matrix degradation onset, min	Matrix onset, interquartile range§	*P* value MT1-MMP vs matrix
Migrating	3	30	2.25	1.50-3.00	0.001	4.50	3.00-6.00	<0.001
Nonmigrating	6	28	1.50	0.75-3.00	<0.001	6.00	3.75-9.00	<0.001

NOTE: The sign and Wilcoxon signed-rank (two-sided) tests were applied for pairwise comparisons between groups.
*Number of independent trials.
†Total number of invadopodia examined.
‡Median values are presented.
§25th and 75th percentile.

associated with activation of integrin-mediated or growth factor–stimulated signaling events (3, 8, 14, 38). Requirements for cortical actin regulators N-WASP and Arp2/3 and their upstream regulators Nck1, Cdc42, and WIP have been shown for epidermal growth factor–stimulated formation of invadopodia in adenocarcinoma cells (14, 39). In addition, the regulators of actin remodeling cofilin, cortactin, Arf6, and dynamin2, which also play roles in membrane trafficking, remodeling, and recycling, localize to invadopodia, and their functional activities are required for invadopodia-mediated matrix degradation (4, 5, 14, 40, 41). Nonetheless, current understanding of molecular mechanisms that govern invadopodia formation has been limited to the early events of actin polymerization induction through the Arp2/3 complex that drives invadopodia initiation (14). In this study, based on an approach that combines the monitoring of the cytoskeletal core of invadopodia with the monitoring of invadopodia function, we substantially extend existing knowledge about the organization and proteolytic function of invadopodia.

While establishing an *in vitro* cell model for invadopodia studies, we found that the expression of wild-type c-Src or a dominant-active c-Src stimulates the formation of invadopodia in breast carcinoma cells. The application of our thin and non-cross-linked fluorescent gelatin matrixes, which provide rapid and sensitive detection of proteolytic activity associated with invadopodia, allowed identification of distinct structural and functional features of invadopodial dynamics. The structural aspect includes the initiation, organization, and stabilization of the F-actin-rich core of invadopodia and invadopodial protrusion extension, all dependent on cortactin, whereas functional activity was associated with the recruitment and organization of proteolytic enzymes at invadopodia that were required for ECM degradation. We found that in MDA-MB-231 carcinoma cells, invadopodial function in gelatin matrix proteolysis required MT1-MMP activity. Down-regulation of MT1-MMP activity blocked matrix degradation but only moderately affected actin/cortactin aggregation of the invadopodia, which otherwise appeared intact, suggesting that dynamic cell-matrix interactions initiate invadopodial actin core formation and dictate protease accumulation at invadopodia. During live-cell imaging, we also observed that only cortactin aggregates at the cell adherence membrane that are destined to become invadopodia initiate MT1-MMP accumulation, indicating the existence of regulatory signaling events yet to be established.

Several studies showed MT1-MMP localization to the migration front of cells in parallel with actin cytoskeleton remodeling when cells are stimulated to migrate. Such reorganization of MT1-MMP has been accompanied by enhancement of MMP-2 activation, showing that MT1-MMP is in an active state at the leading edge (42–44). In this study, we revealed that MT1-MMP, although present over the entire plasma membrane, is specifically concentrated at the invadopodia of carcinoma cells and promotes matrix degradation at these sites. MDA-MB-231 cells plated on gelatin matrix and labeled for FAK or paxillin, in addition to invadopodia, show the formation of focal adhesions that do not overlap with invadopodial structures or degradation sites (data not shown). We speculate that focal adhesions, by providing the main sites of cell adhesion to ECM and sites of signal transduction into the cell interior, might support local membrane attachment to permit initiation and extension of invadopodia into the matrix. The proteolytic activity accumulated at invadopodial tips degrades the ECM and promotes invasion by weakening matrix resistance.

Some cell types engaged in matrix remodeling and tissue invasion form podosomes, actin-rich adhesion structures that share many

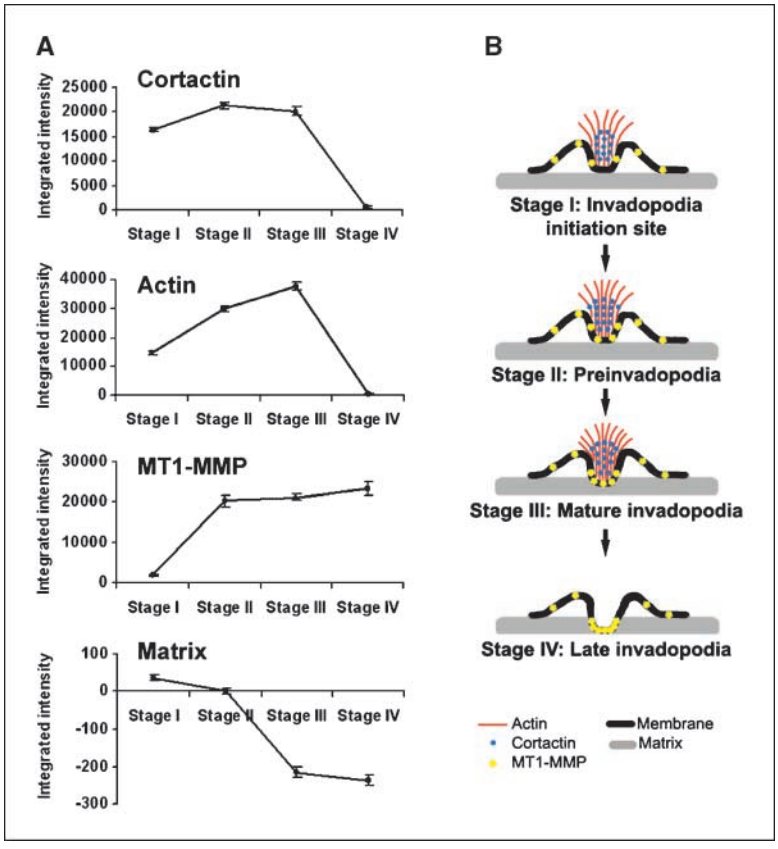

Figure 6. Stepwise model of invadopodia assembly and function. *A,* estimated levels of cortactin, actin, and MT1-MMP at invadopodia and the degree of matrix degradation quantified for each invadopodial stage. Y527F c-Src MDA-MB-231 cells stably expressing MT1-MMP-eGFP were incubated on gelatin-Alexa568 matrices for 45 minutes, 1 hour, 2 hours, or 3 hours. At the end of each incubation period, cells were fixed/permeabilized and immunolabeled for cortactin (4F11 antibody followed by Cy5-conjugated secondary staining) and actin (phalloidin-rhodamine). Confocal image stacks of gelatin-Alexa568 and phalloidin-rhodamine were acquired using the META detector. Dye separation was done according to the Zeiss linear unmixing algorithm. Intensity profiles for cortactin, actin, MT1-MMP, and matrix for single invadopodia were obtained from line scans of fluorescent images. The fluorescence intensities were analyzed with Origin software (OriginLab, Northampton, MA). For each stage, 25 to 30 invadopodia were analyzed. *B,* schematic representation of four stages of invadopodia formation and function.

molecular components with invadopodia (45, 46). The classic podosome structure is a circular F-actin core surrounded by a ring of vinculin. In contrast, ~95% of the invadopodia of c-Src-expressing carcinoma cells plated on gelatin matrix and labeled for actin and vinculin lack vinculin-rich rings (data not shown). Thus, invadopodia of MDA-MB-231 cells are distinct from classic podosomes.

In summary, based on the results of examination of cells at different time points, live-cell imaging, and fluorescence intensity analysis, we have identified a stepwise mechanism of invadopodia formation and function (Fig. 6*B*). Invadopodia start as an invadopodial initiation site by accumulation of actin and cortactin at areas of cell membrane adherence to ECM. The onset of MT1-MMP accumulation defines the full-fledged preinvadopodia stage. This stage involves ongoing increases in the amounts of actin and cortactin along with the increase in MT1-MMP. The beginning of matrix degradation defines the formation of mature invadopodia, which are enriched in actin, cortactin, and MT1-MMP. The dispersal of F-actin and cortactin from mature invadopodia results in the formation of late invadopodia, which remain enriched in MT1-MMP capable of continuing focal degradation.

Acknowledgments

Received 6/21/2005; revised 1/10/2006; accepted 1/18/2006.

The costs of publication of this article were defrayed in part by the payment of page charges. This article must therefore be hereby marked *advertisement* in accordance with 18 U.S.C. Section 1734 solely to indicate this fact.

References

1. Basbaum CB, Werb Z. Focalized proteolysis: spatial and temporal regulation of extracellular matrix degradation at the cell surface. Curr Opin Cell Biol 1996;8:731–8.

2. Chen WT. Proteolytic activity of specialized surface protrusions formed at rosette contact sites of transformed cells. J Exp Zool 1989;251:167–85.

3. Coopman PJ, Do MT, Thompson EW, Mueller SC. Phagocytosis of cross-linked gelatin matrix by human breast carcinoma cells correlates with their invasive capacity. Clin Cancer Res 1998;4:507–15.

4. Bowden ET, Barth M, Thomas D, Glazer RI, Mueller SC. An invasion-related complex of cortactin, paxillin and PKCμ associates with invadopodia at sites of extracellular matrix degradation. Oncogene 1999;18:4440–9.

5. Baldassarre M, Pompeo A, Beznoussenko G, et al. Dynamin participates in focal extracellular matrix degradation by invasive cells. Mol Biol Cell 2003;14:1074–84.

6. Buccione R, Orth JD, McNiven MA. Foot and mouth: podosomes, invadopodia and circular dorsal ruffles. Nat Rev Mol Cell Biol 2004;5:647–57.

7. Wang W, Goswami S, Sahai E, Wyckoff JB, Segall JE, Condeelis JS. Tumor cells caught in the act of invading: their strategy for enhanced cell motility. Trends Cell Biol 2005;15:138–45.

8. Mueller SC, Ghersi G, Akiyama SK, et al. A novel protease-docking function of integrin at invadopodia. J Biol Chem 1999;274:24947–52.

9. Monsky WL, Lin CY, Aoyama A, et al. A potential marker protease of invasiveness, seprase, is localized on invadopodia of human malignant melanoma cells. Cancer Res 1994;54:5702–10.

10. Nakahara H, Howard L, Thompson EW, et al. Transmembrane/cytoplasmic domain-mediated membrane type 1-matrix metalloprotease docking to invadopodia is required for cell invasion. Proc Natl Acad Sci U S A 1997;94:7959–64.

11. Monsky WL, Kelly T, Lin CY, et al. Binding and localization of M(r) 72,000 matrix metalloproteinase at cell surface invadopodia. Cancer Res 1993;53:3159–64.

12. Artym VV, Kindzelskii AL, Chen WT, Petty HR. Molecular proximity of seprase and the urokinase-type plasminogen activator receptor on malignant melanoma cell membranes: dependence on β_1 integrins and the cytoskeleton. Carcinogenesis 2002;23:1593–601.

13. Chen WT. Proteases associated with invadopodia, and their role in degradation of extracellular matrix. Enzyme Protein 1996;49:59–71.

14. Yamaguchi H, Lorenz M, Kempiak S, et al. Molecular mechanisms of invadopodium formation: the role of the N-WASP-Arp2/3 complex pathway and cofilin. J Cell Biol 2005;168:441–52.

15. Weed SA, Parsons JT. Cortactin: coupling membrane dynamics to cortical actin assembly. Oncogene 2001;20:6418–34.

16. Daly RJ. Cortactin signalling and dynamic actin networks. Biochem J 2004;382:13–25.

17. Weaver AM, Karginov AV, Kinley AW, et al. Cortactin promotes and stabilizes Arp2/3-induced actin filament network formation. Curr Biol 2001;11:370–4.

18. Cao H, Weller S, Orth JD, et al. Actin and Arf1-dependent recruitment of a cortactin-dynamin complex to the Golgi regulates post-Golgi transport. Nat Cell Biol 2005;7:483–92.

19. Martinez-Quiles N, Ho HY, Kirschner MW, Ramesh N, Geha RS. Erk/Src phosphorylation of cortactin acts as a switch on-switch off mechanism that controls its ability to activate N-WASP. Mol Cell Biol 2004;24:5269–80.

20. Schuuring E. The involvement of the chromosome 11q13 region in human malignancies: cyclin D1 and EMS1 are two new candidate oncogenes—a review. Gene 1995;159:83–96.

21. Patel AS, Schechter GL, Wasilenko WJ, Somers KD. Overexpression of EMS1/cortactin in NIH3T3 fibroblasts causes increased cell motility and invasion *in vitro*. Oncogene 1998;16:3227–32.

22. Huang C, Liu J, Haudenschild CC, Zhan X. The role of tyrosine phosphorylation of cortactin in the locomotion of endothelial cells. J Biol Chem 1998;273:25770–6.

23. Chuma M, Sakamoto M, Yasuda J, et al. Overexpression of cortactin is involved in motility and metastasis of hepatocellular carcinoma. J Hepatol 2004;41:629–36.

24. Li Y, Tondravi M, Liu J, et al. Cortactin potentiates bone metastasis of breast cancer cells. Cancer Res 2001;61:6906–11.

25. Itoh Y, Seiki M. MT1-MMP: an enzyme with multidimensional regulation. Trends Biochem Sci 2004;29:285–9.

26. Holmbeck K, Bianco P, Caterina J, et al. MT1-MMP-deficient mice develop dwarfism, osteopenia, arthritis, and connective tissue disease due to inadequate collagen turnover. Cell 1999;99:81–92.

27. Seiki M, Yana I. Roles of pericellular proteolysis by membrane type-1 matrix metalloproteinase in cancer invasion and angiogenesis. Cancer Sci 2003;94:569–74.

28. Hotary KB, Allen ED, Brooks PC, Datta NS, Long MW, Weiss SJ. Membrane type I matrix metalloproteinase usurps tumor growth control imposed by the three-dimensional extracellular matrix. Cell 2003;114:33–45.

29. Sabeh F, Ota I, Holmbeck K, et al. Tumor cell traffic through the extracellular matrix is controlled by the membrane-anchored collagenase MT1-MMP. J Cell Biol 2004;167:769–81.

30. Myoui A, Nishimura R, Williams PJ, et al. C-SRC tyrosine kinase activity is associated with tumor colonization in bone and lung in an animal model of human breast cancer metastasis. Cancer Res 2003;63:5028–33.

31. Liu S, Netzel-Arnett S, Birkedal-Hansen H, Leppla SH. Tumor cell-selective cytotoxicity of matrix metalloproteinase-activated anthrax toxin. Cancer Res 2000;60:6061–7.

32. Remacle A, Murphy G, Roghi C. Membrane type I-matrix metalloproteinase (MT1-MMP) is internalised by two different pathways and is recycled to the cell surface. J Cell Sci 2003;116:3905–16.

33. Jacobs C, Rubsamen H. Expression of pp60c-src protein kinase in adult and fetal human tissue: high activities in some sarcomas and mammary carcinomas. Cancer Res 1983;43:1696–702.

34. Rosen N, Bolen JB, Schwartz AM, Cohen P, DeSeau V, Israel MA. Analysis of pp60c-src protein kinase activity in human tumor cell lines and tissues. J Biol Chem 1986;261:13754–9.

35. Verbeek BS, Vroom TM, Adriaansen-Slot SS, et al. c-Src protein expression is increased in human breast cancer. An immunohistochemical and biochemical analysis. J Pathol 1996;180:383–8.

36. Egan C, Pang A, Durda D, Cheng HC, Wang JH, Fujita DJ. Activation of Src in human breast tumor cell lines: elevated levels of phosphotyrosine phosphatase activity that preferentially recognizes the Src carboxy terminal negative regulatory tyrosine 530. Oncogene 1999;18:1227–37.

37. Webster MA, Cardiff RD, Muller WJ. Induction of mammary epithelial hyperplasias and mammary tumors in transgenic mice expressing a murine mammary tumor virus/activated c-src fusion gene. Proc Natl Acad Sci U S A 1995;92:7849–53.

38. Nakahara H, Mueller SC, Nomizu M, Yamada Y, Yeh Y, Chen WT. Activation of β1 integrin signaling stimulates tyrosine phosphorylation of p190RhoGAP and membrane-protrusive activities at invadopodia. J Biol Chem 1998;273:9–12.

39. Nakahara H, Otani T, Sasaki T, Miura Y, Takai Y, Kogo M. Involvement of Cdc42 and Rac small G proteins in invadopodia formation of RPMI7951 cells. Genes Cells 2003;8:1019–27.

40. Tague SE, Muralidharan V, D'Souza-Schorey C. ADP-ribosylation factor 6 regulates tumor cell invasion through the activation of the MEK/ERK signaling pathway. Proc Natl Acad Sci U S A 2004;101:9671–6.

41. Hashimoto S, Onodera Y, Hashimoto A, et al. Requirement for Arf6 in breast cancer invasive activities. Proc Natl Acad Sci U S A 2004;101:6647–52.

42. Itoh Y, Takamura A, Ito N, et al. Homophilic complex formation of MT1-MMP facilitates proMMP-2 activation on the cell surface and promotes tumor cell invasion. EMBO J 2001;20:4782–93.

43. Galvez BG, Matias-Roman S, Albar JP, Sanchez-Madrid F, Arroyo AG. Membrane type 1-matrix metalloproteinase is activated during migration of human endothelial cells and modulates endothelial motility and matrix remodeling. J Biol Chem 2001;276:37491–500.

44. Lehti K, Valtanen H, Wickstrom SA, Lohi J, Keski-Oja J. Regulation of membrane-type-1 matrix metalloproteinase activity by its cytoplasmic domain. J Biol Chem 2000;275:15006–13.

45. Linder S, Aepfelbacher M. Podosomes: adhesion hotspots of invasive cells. Trends Cell Biol 2003;13:376–85.

46. Osiak AE, Zenner G, Linder S. Subconfluent endothelial cells form podosomes downstream of cytokine and RhoGTPase signaling. Exp Cell Res 2005;307:342–53.